RSC Advances

PAPER

View Article Online
View Journal | View Issue

Cite this: *RSC Adv.*, 2021, **11**, 37584

Chiral fluorescence recognition of glutamine enantiomers by a modified Zr-based MOF based on solvent-assisted ligand incorporation†

Qin Shili, Sun Yangyang, He Xudong, Chu Hongtao, Gao Lidi,* Hou Zhongyu, Zhao Dongsheng, Liu Xinyao and Zhou Sibing

In this study, three types of chiral fluorescent zirconium-based metal–organic framework materials were synthesized using L-dibenzoyl tartaric acid as the chiral modifier by the solvent-assisted ligand incorporation method, which was the porous coordination network yellow material, denoted as PCN-128Y. PCN-128Y-1 and PCN-128Y-2 featured unique chiral selectivity for the Gln enantiomers amongst seven acids and the highly stable luminescence property, which were caused by the heterochiral interaction and aggregation-induced emission. Furthermore, a rapid fluorescence method for the chiral detection of glutamine (Gln) enantiomers was developed. The homochiral crystals of PCN-128Y-1 displayed enantiodiscrimination in the quenching by D-Gln such that the ratio of enantioselectivity was 2.0 in 30 seconds at pH 7.0, according to the Stern–Volmer quenching plots. The detection limits of D- and L-Gln were 6.6 × 10^{-4} mol L^{-1} and 3.3 × 10^{-4} mol L^{-1}, respectively. Finally, both the maximum adsorption capacities of PCN-128Y-1 for the Gln enantiomers ($Q_{e(L\text{-}Gln)}$ = 967 mg g^{-1}; $Q_{e(D\text{-}Gln)}$ = 1607 mg g^{-1}) and the enantiomeric excess value (6.2%) manifested that PCN-128Y-1 had strong adsorption capacity for the Gln enantiomers and higher affinity for D-Gln.

Received 13th September 2021
Accepted 20th October 2021

DOI: 10.1039/d1ra06857a

rsc.li/rsc-advances

Introduction

Chirality is one of the most important characteristics of nature or life process,[1–3] and chiral compounds are widely used in many areas. Amino acids are also chiral and only their L forms are of relevance in living organisms.[4,5] Glutamine (Gln), as an encoded amino acid, is not only a critical respiratory fuel but is also utilized for the fast multiplication of cells from tumoral tissues.[6,7] Importantly, similar to a majority of the chiral compounds, there is a significant difference between enantiomeric forms of Gln in their biological activities and transport pathways.[8,9] Yet, a lack of enantiomer recognition has existed for many years, *e.g.*, the kits commonly used in the market are not enantioselective; thus, the term Gln only represents L-Gln. In fact, the DNA of gastric cancer patients also could produce D-Gln.[10] As a result, it is necessary to recognize and measure the single enantiomer in the pharmaceutical and biochemical fields. The significant methods for chiral recognition are various detection methods and chiral probes.[11]

Compared with the other conventional methods, such as chiral electrophoresis, chiral chromatography, and enzymatic methods, fluorescence, as a rapid enantiodiscrimination method, has drawn special attention because of its advantages of high sensitivity, affordable instruments, and multiple detection modes.[12–16]

Metal–organic frameworks (MOFs) are a novel class of advanced materials with porous networks composed of organic ligands and metal ions or clusters. Their large surface areas, diverse structures, and functions endow them potential for diverse applications.[17–19] Notably, luminescent metal–organic frameworks (LMOFs) with aromatic subunits have been widely developed as chemical sensors for various targets,[20–22] such as metal cations,[23,24] small molecules,[25,26] gases,[27] biomarkers,[28,29] pH,[30,31] and temperature.[32] The most common form of signal transduction in LMOFs is quenching, or occasionally, the enhancement of photo-induced emission due to guest adsorption. PCN-128, as a piezoelectric LMOF, is constructed from H_4ETTC (4′,4‴,4⁗,4⁗′′′-(ethene-1,1,2,2-tetrayl) tetrakis-(([1,1′-biphenyl]-4-carboxylic acid))) and eight-connected Zr_6 clusters and has high reversibility, coordinated luminescence, and a stable structure. PCN-128Y is a high-temperature activated form of PCN-128, which exhibits a wide hexagonal channel and stable fluorescence properties (PCN stands for metal coordination network, Y stands for yellow).[33] Zhou[34] has examined the detection and removal of antibiotics in water based on the efficient photoluminescence quenching of tetracycline by PCN-128Y. Furthermore, the terminal –OH/H_2O groups between the Zr_6 cluster nodes of PCN-128Y could be substituted with structural or nonstructural organic ligands featuring charge-

College of Chemistry and Chemical Engineering, Qiqihar University, Qiqihar, Heilongjiang, 161006, P. R. China. E-mail: gaolidi@163.com; Tel: +86 0452 2738214

† Electronic supplementary information (ESI) available. See DOI: 10.1039/d1ra06857a

compensating groups by solvent-assisted ligand incorporation (SALI), which is a mild interior decoration method. After the incorporation of the nonstructural organic ligand, the secondary modifications of this ligand may be conducted in order to access otherwise unattainable functionalities.[35,36] It is noteworthy that chiral metal–organic frameworks (CMOFs) with both the intrinsic features of MOFs and the chiral recognition sites could be obtained by a post-synthetic modification method.[37–39] However, few studies on the highly selectivity as well as enantiodiscrimination by chiral fluorescence Zr-MOF have been reported.

L-DBTarA as a chiral selector is a benzoyl derivative of L-tartaric acid and is widely used in chiral separation and recognition.[40] The aim of this paper is to provide methods to prepare the modified PCN-128Y using L-DBTarA as the chiral selector by the SALI method. Furthermore, the fluorescence properties, chiral recognition ability, interaction mechanism, and adsorption capacity of chiral modified PCN-128Y were further explored. Finally, a rapid and reliable method for the chiral fluorescence detection of Gln enantiomers was developed.

Experiment

Materials and methods

The chemicals used in the experiment were all obtained from commercial sources and used without further purification. Anhydrous zirconium chloride ($ZrCl_4$) and L-dibenzoyl tartaric acid (L-DBTarA) were purchased from Beijing Yinuokai Technology Co., Ltd. (Beijing, China), and H_4ETTC (4′,4‴,4⁗,4⁗′-(ethene-1,1,2,2-tetrayl)tetrakis-(([1,1′-biphenyl]-4-carboxylic acid))) was purchased from Shanghai Tengqian Biological Technology Co., Ltd. (Shanghai, China). Scanning electron microscopy (SEM) was carried out using a TM-3000 scanning electron microscope. Powder X-ray diffraction (XRD) measurements were collected on a Smart Lab X-ray diffractometer using Cu-K/Alpha radiation in the 2θ range of 2–20°. N_2 adsorption–desorption and pore size distribution (BET) were measured with a Micromeritics 3 Flex instrument. The samples were vacuum-pretreated at 150 °C and N_2 was used as the adsorbent for adsorption and desorption experiments at −196 °C. The Fourier transform infrared (FT-IR) spectra were obtained on a Spotlight 400 FT-IR spectrophotometer. Thermogravimetric analysis (TG) was performed on a STA 449 F3 Jupiter apparatus under N_2 from room temperature to 800 °C at a heating rate of 5 °C min^{-1}. The fluorescence spectra were measured on a LS55 Fluorescence spectrophotometer at room temperature.

Synthesis of chiral modified PCN-128Y

First and foremost, the preparation method of PCN-128Y was adapted from that reported in the previous literature.[33,34] The second step was the preparation of chiral modified PCN-128Y. The carboxyl group with charge compensation in L-DBTarA was used to substitute the aqua/hydroxo pair on the PCN-128Y metal cluster node to achieve the purpose of modification. PCN-128Y (30 mg) and L-DBTarA were dispersed in 3.0 mL nitrogen dimethyl formamide (DMF) and put into a 5 mL Pyrex vial, then sealed and heated at 60 °C for 24 hours. The final product was washed multiple times with DMF and acetone, then collected by centrifugation and dried at 60 °C in a vacuum oven. Three types of chiral modified PCN-128Y were synthesized according to the different molar ratios of PCN-128Y to L-DBTarA at 1 : 2, 1 : 4, and 1 : 10, and named as PCN-128Y-1, PCN-128Y-2, and PCN-128Y-3, respectively.

Fluorescence measurements and chiral recognition

The fluorescence and chiral recognition properties of the synthesized PCN-128Y and three types of chiral modified PCN-128Y were studied, respectively. Investigation on the luminescent properties were undertaken with PCN-128Y as an example. In a typical experimental device, 1 mg PCN-128Y powder was accurately weighed and ultrasonically dispersed for 30 seconds in 20 mL ultrapure water. 2.0 mL of the suspension was taken in a quartz colorimetric cell and the excitation wavelength of the fluorescence measurements was 325 nm.

PCN-128Y and chiral modified PCN-128Y were used for the chiral fluorescence recognition of Gln enantiomers. The investigation on chiral recognition was undertaken with PCN-128Y-1 as an example. 2.0 mL uniform PCN-128Y-1 aqueous solution (0.05 mg mL^{-1}) was mixed with 50 μL 1 mol L^{-1} D- or L-Gln enantiomer solution and ultrasonicated for 30 seconds. The factors influencing the chiral recognition by PCN-128Y-1 of the Gln enantiomers were studied at an optimal excitation wavelength 325 nm. The chiral recognition experiments under the same conditions were carried out by PCN-128Y, PCN-128Y-2, and PCN-128Y-3. Meanwhile, experiments on the chiral selectivity were carried out using D/L-phenylalanine (D/L-Phe), D/L-valine (D/L-Val), D/L-alanine (D/L-Ala), D/L-proline (D/L-Pro), D/L-tyrosine (D/L-Tyr), and D/L-tryptophan (D/L-Trp) as the reference adsorption substrates.

Chiral adsorption performance of PCN-128Y-1

The chiral adsorption performance of PCN-128Y-1 was investigated after the above experiments. Ultraviolet spectroscopy and capillary electrophoresis were used for the determination of the adsorption capacity (Q_e) and the enantiomeric excess value (e.e.%), respectively.

In the isothermal adsorption experiment, 1.0 mg PCN-128Y-1 was added to 10 mL of an aqueous solution of L- or D-Gln with various concentrations ranging from 0.1 to 5.0 mmol L^{-1}. The mixture was incubated for 12 h at room temperature after ultrasonication. The supernatants and PCN-128Y-1 were isolated by a 0.45 μm filter membrane, and then the concentrations of the single Gln enantiomer before and after adsorption were measured by an ultraviolet spectrometer. Q_e was calculated according to the following equation.[41]

$$Q_e = \frac{C_0 - C_e}{m} \times V$$

where C_0 and C_e are the initial and equilibrium adsorption concentrations of the analytes in the aqueous solution, while V and m are the volume of the solution and the mass of PCN-128Y-1, respectively.

In the capillary electrophoresis experiment, 1.0 mg of PCN-128Y-1 was added to 10 mL of the mixed aqueous solution of Gln enantiomers and incubated for 12 h at room temperature after ultrasonication. The supernatants were isolated with a 0.45 μm filter membrane and analyzed by capillary electrophoresis. The chromatographic conditions were optimized on a Bekman PA800 Plus separation system equipped with an ultraviolet detector using 15 mmol L^{-1} hydroxypropyl-β-cyclodextrin as a chiral additive and pH = 7 20 mmol L^{-1} phosphate as the buffer solution. The separation voltage and temperature were 20 kV and 30 °C, respectively. The injection time and voltage were set to 10 kV and 5 seconds, respectively. A fused silica capillary with dimensions of 50 μm id and effective length of 40 cm was used for the separation of the analytes. The e.e.% was calculated by the following formula,[42] where A_D and A_L represent the peak areas of D- and L-Gln, respectively.

$$\text{e.e.}\% = \left|\frac{A_L - A_D}{A_L + A_D}\right| \times 100\%$$

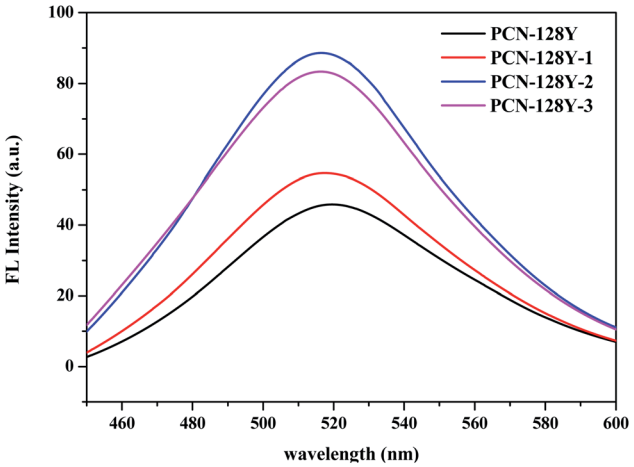

Fig. 2 Fluorescence spectra of PCN-128Y and PCN-128Y-1, 2, 3 (PCN-128Y-1, 2, 3 represents the different molar ratios of PCN-128Y to L-DBTarA at 1 : 2, 1 : 4, and 1 : 10. Experimental conditions: 0.05 mg mL^{-1} MOFs, 30 seconds incubation time, and 325 nm excitation wavelength).

Results and discussion

Preparation and characterization of chiral modified PCN-128Y

SALI is a post-synthetic modification strategy, which refers to the combination of metal clusters and unbridged ligands. The metal clusters, bridged groups, and modified groups could be connected in order to be secondarily functionalized through the binding part.[43,44] As shown in Fig. 1, the carboxyl group with charge compensation in L-DBTarA was used to substitute the aqua/hydroxo pair of the PCN-128Y metal cluster node to achieve the purpose of modification.[39,43,44] The chiral recognition sites were successfully introduced into the fluorescence MOFs for the enantiodiscrimination of amino acids.

The photoluminescence spectra of PCN-128Y and PCN-128Y-1, 2, 3 aqueous suspensions were studied at the optimum excitation wavelength of 325 nm, as shown in Fig. 2. Four kinds of MOFs exhibited a strong and wide emission band centered at 518 nm, which could be attributed to the π–π* electron transition of the H_4ETTC ligands. The fluorescence intensity first increased and then decreased with the increasing amount of the chiral modifier L-DBTarA.

Meanwhile, the quantum yield of PCN-128Y and PCN-128Y-1, 2, 3 was measured using rhodamine 6G as the reference standard material (Y_s = 95%) under 325 nm excitation wavelength. Then, the quantum yield results were calculated by the following formula; the specific data is shown in Table 1.[45]

Table 1 Measurements of the fluorescence quantum yield of PCN-128Y and PCN-128Y-1, 2, 3

Types	As	Fs	Ys	Au	Fu	Yu
PCN-128Y	0.030	1850.34	95%	0.026	1271.73	75.3%
PCN-128Y-1	0.030	1850.34	95%	0.033	1686.15	78.7%
PCN-128Y-2	0.030	1850.34	95%	0.035	1986.03	87.4%
PCN-128Y-3	0.030	1850.34	95%	0.036	1998.37	85.5%

$$Y_u = \frac{Y_s F_u}{F_s}\frac{A_s}{A_u}$$

where Y_u and Y_s are the fluorescence quantum yields of the test substance and the reference standard substance, F_u and F_s are the integrated fluorescence intensity of the test substance and the reference standard substance, and A_u and A_s are the absorbance at the excitation wavelength of the test substance and the reference standard substance, respectively.

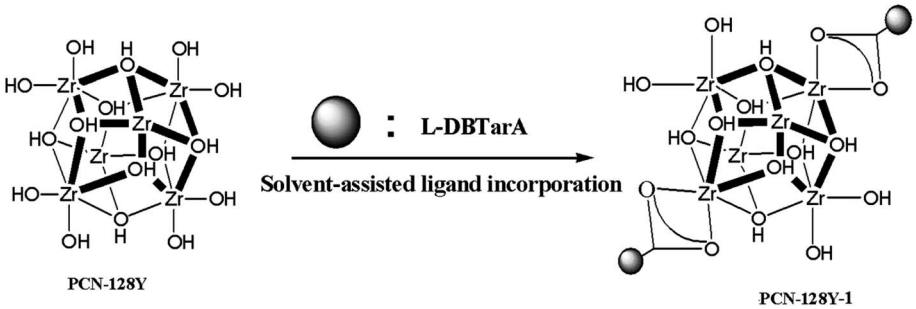

Fig. 1 Synthetic mechanism of PCN-128Y-1 by SALI.

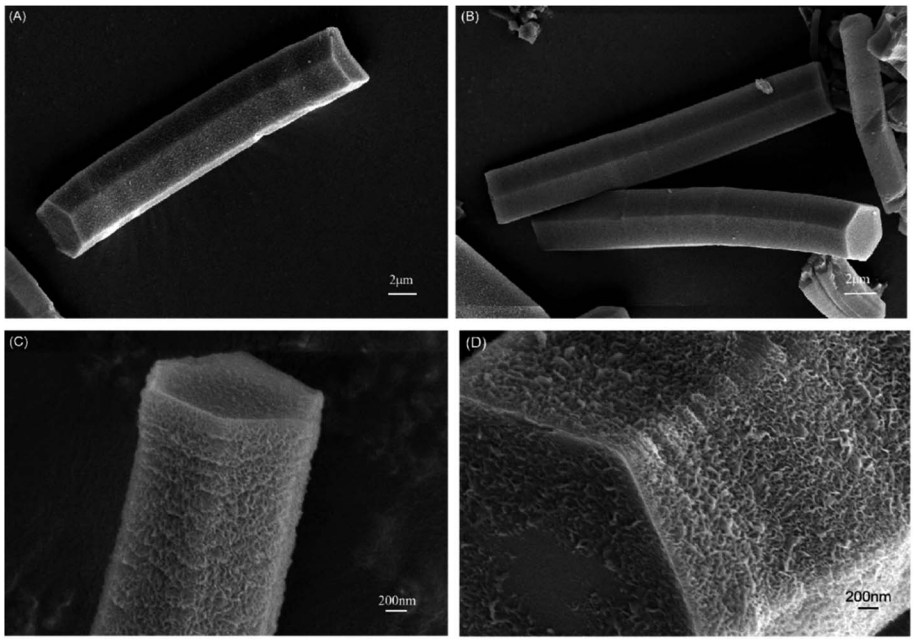

Fig. 3 SEM characterization images of PCN-128Y (A and C) and PCN-128Y-1 (B and D).

The quantum yields of PCN-128Y-1, PCN-128Y-2, and PCN-128Y-3 were 78.7%, 87.4%, and 85.5%, respectively, which were higher than that of PCN-128Y (75.3%) due to the phenomenon of aggregation-induced emission.[46,47] When the chiral modifier L-DBTarA was introduced, the π–π* conjugated system in the framework of the MOFs was expanded, and the rotation and vibration of the benzene ring were more inhibited and the non-radiative transition was reduced, thereby resulting in an increase in the fluorescence intensity. However, as the molar ratio of PCN-128Y and L-DBTarA increased to 1 : 10, the fluorescence intensity of PCN-128Y-3 decreased. It may be that the excessive amount of the organic chiral modifier deteriorated its crystallinity, which was consistent with the results of XRD (Fig. S1†). In summary, the four kinds of chiral modified PCN-128Y had outstanding photoluminescence properties.

The quintessential examples of PCN-128 and PCN-128Y-1 were chosen for a series of characterization. The size and morphology of PCN-128Y and PCN-128Y-1 were studied using SEM. As shown in Fig. 3, both PCN-128Y (Fig. 3(A)) and PCN-128Y-1 (Fig. 3(B)) have regular six-prismatic crystals, and the mean side length and height of the hexagon was approximately 600 nm and 22 μm, respectively. Meanwhile, the surface of PCN-128Y (Fig. 3(C)) and PCN-128Y-1 (Fig. 3(D)) exhibited characteristics of porosity under the magnification condition, which was beneficial for improving the transmission speed of the adsorbate and reducing the response time. By comparing the SEM images of PCN-128Y before and after the modification reaction, it could be seen that the introduction of the chiral modifier did not alter its particle size, morphology, and crystal structure.

The FT-IR spectra of PCN-128Y and PCN-128Y-1 further demonstrated the successful preparation of PCN-128Y-1. As an illustration, the typical infrared absorption peaks of PCN-128Y were the stretching vibration of the carboxylic carbonyl group at 1696 cm^{-1}, the skeleton vibration absorption peak of the benzene ring at 1605, 1530, and 1416 cm^{-1}, and the stretching vibration absorption peak of Zr–O at 651 cm^{-1} in curve (a) of Fig. 4. Compared with PCN-128Y, the absorption peaks of 1699, 1607, 1531, 1417, and 650 cm^{-1} were not only preserved in PCN-128Y-1 but a new vibration absorption peak of the anhydride group also appeared and generated a bathochromic shift to 1652 cm^{-1} because of the formation of a conjugated delocalized π-bond between L-DBTarA and H_4ETTC ligands. Then, the ester group absorption of C–O–C at 1282, 1181, and 1109 cm^{-1} were also stronger. The above results indicated that PCN-128Y was chiral modified successfully.

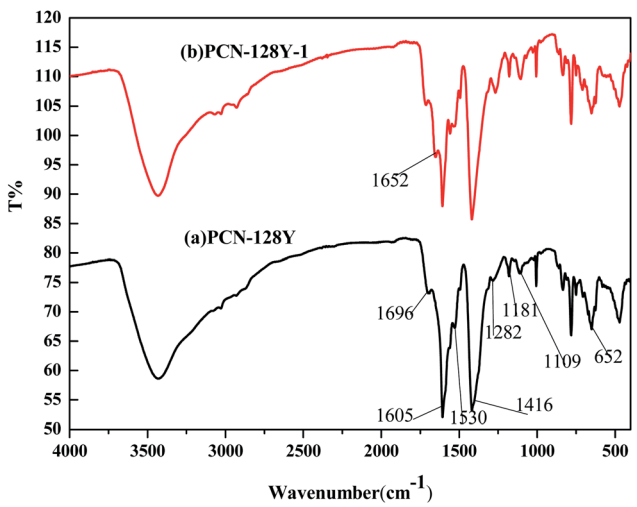

Fig. 4 FT-IR spectra of PCN-128Y and PCN-128Y-1.

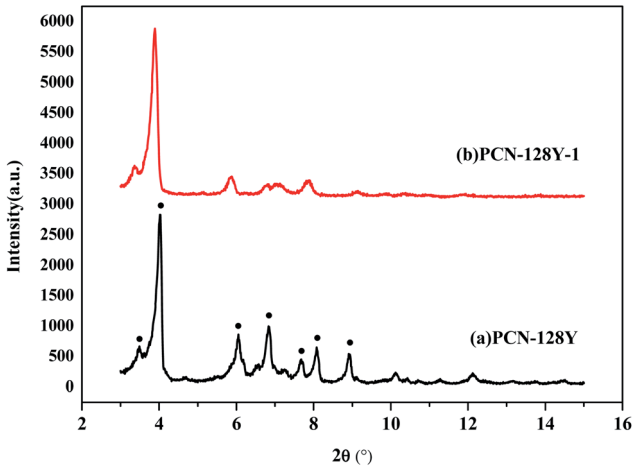

Fig. 5 XRD characterization of PCN-128Y and PCN-128Y-1.

The crystal structure of both PCN-128Y and PCN-128Y-1 was characterized with XRD, as shown in Fig. 5. The results showed that PCN-128Y had diffraction peaks of different intensities at the 2θ angles of 3.4°, 3.9°, 6.0°, 6.8°, 7.6°, 8.0°, and 8.9°, which were basically consistent with the diffraction peaks reported in the previous study.[33] Also, the diffraction peak intensity and position of PCN-128Y-1 were in accordance with that of PCN-128Y, which demonstrated that the synthesized MOFs had a regular crystal structure and was not changed by the chiral modifier L-DBTarA. However, with the increase in the chiral modifier content, the diffraction peak intensity of synthesized chiral modified PCN-128Y decreased and broadened in Fig. S1.†

The thermal stability of PCN-128Y and PCN-128Y-1 were characterized by TG and are shown in Fig. 6. The weight loss processes of PCN-128Y and PCN-128Y-1 were separated into two and three stages, respectively. The first stage in the temperature range of 20 °C to 200 °C was due to the loss of absorbed water and solvent. The second stage of PCN-128Y began at 450 °C, which represented the collapse of the PCN-128Y framework. It was noticed that there was one more weight loss stage of PCN-128Y-1 because of the decomposition of the chiral modifier L-DBTarA in the range of 200 °C to 500 °C. The same results were observed in Fig. S2,† which exhibited the TG characterization diagrams of PCN-128Y and PCN-128Y-1, 2, 3. Compared with PCN-128Y, the frameworks of the three kinds of the chiral modified PCN-128Y collapsed after 500 °C, which indicated that the introduction of chiral modifiers enhanced the degree of conjugation in MOFs system, thereby improving the thermal stability of MOFs.

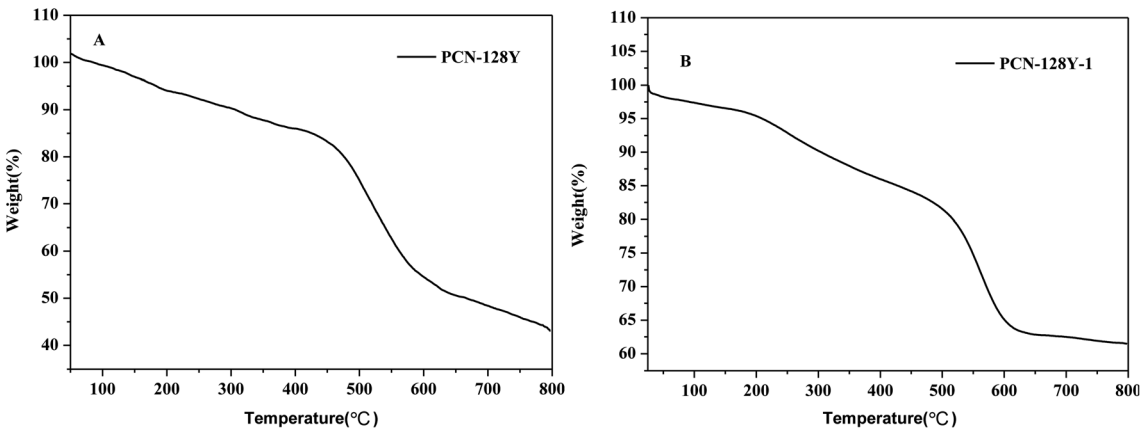

Fig. 6 TG characterization curves of PCN-128Y and PCN-128Y-1.

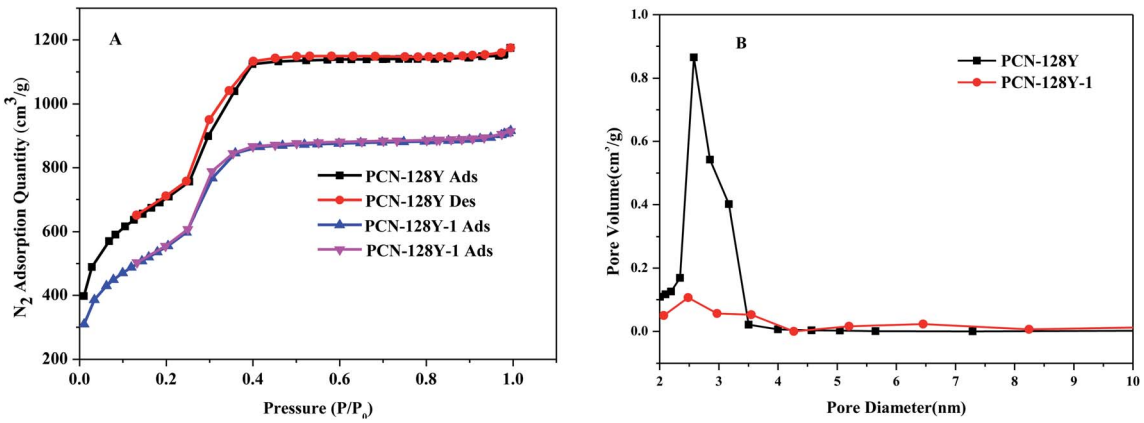

Fig. 7 N_2 adsorption and desorption isotherm (A) and pore size distribution diagram (B) of PCN-128Y and PCN-128Y-1.

Table 2 Specific surface areas, average pore sizes, and pore volumes of PCN-128Y and PCN-128Y-1

Sample	BET ($m^2\ g^{-1}$)	D (nm)	V ($cm^3\ g^{-1}$)
PCN-128Y	2428	2.5647	0.8600
PCN-128Y-1	1852	2.5147	0.1063

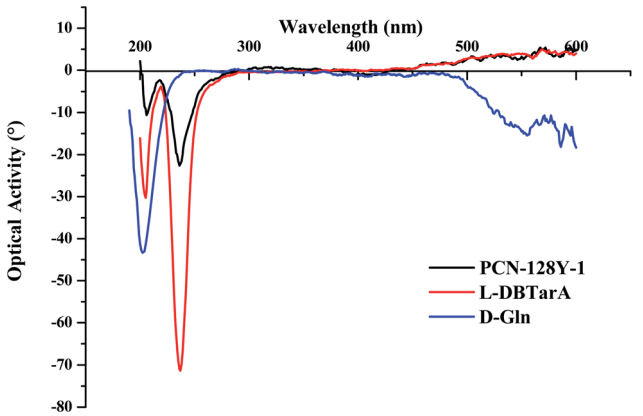

Fig. 8 The circular dichroism spectra of PCN-128Y-1, L-DBTarA, and D-Gln.

The pore properties of the prepared materials were characterized by BET analysis shown in Fig. 7. The curves of PCN-128Y and PCN-128Y-1 were assigned to the type IV adsorption isotherms and the retention loop with relative pressure (P/P_0) of 0.24–0.41 indicated the presence of mesopores. The pore sizes of PCN-128Y and PCN-128Y-1 were mainly 2.6 nm and 2.5 nm, respectively, as shown in Fig. 7(B). Moreover, compared with PCN-128Y, the surface area and pore volume of PCN-128Y-1 decreased because of the introduction of the chiral modifier into PCN-128Y, as shown in Table 2.

The circular dichroism characterization of PCN-128Y-1, L-DBTarA, and D-Gln is shown in Fig. 8. The optical activities of PCN-128Y-1, L-DBTarA, and D-Gln were measured to be −21.0°, −71.1°, and −42.9°, respectively, which showed the same negative optical rotation.

Chiral fluorescence recognition of Gln enantiomers

Gln, an encoded and important amino acid, was chosen as the probe chiral molecule to evaluate the fluorescence enantiodiscrimination of PCN-128Y and PCN-128Y-1, 2, 3. In the first place, the fluorescence intensity of four types of MOFs was quenched by both D- and L-Gln, which was attributed to photoelectron transfer (PET), as shown in Fig. 9(A)–(D). As for PET, when the fluorophore was excited, the electronic hole generated by electron transition could be filled by an electron in the fluorophore's ground state, which

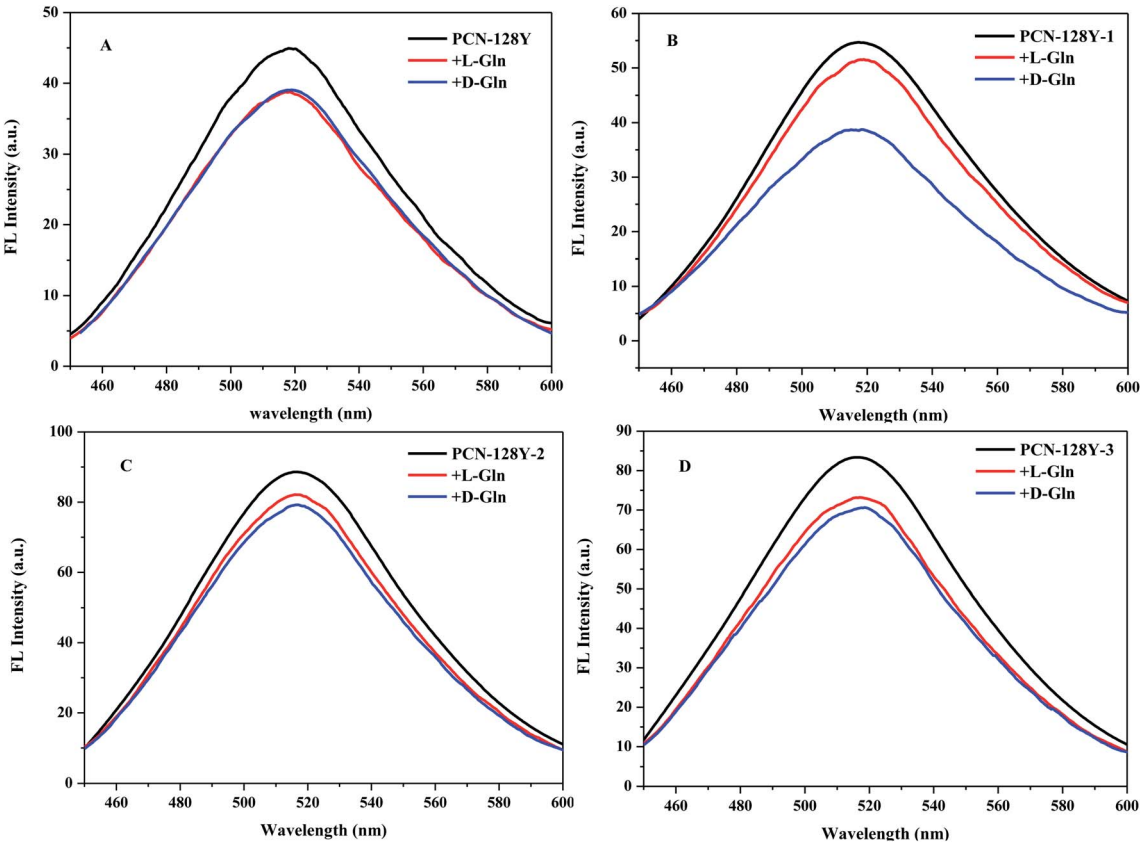

Fig. 9 Chiral fluorescence spectra of PCN-128Y (A), PCN-128Y-1 (B), PCN-128Y-2 (C), and PCN-128Y-3 (D) quenched by L/D-Gln (experimental conditions: 0.05 mg mL^{-1} MOFs, 50 μL 1 mol L^{-1} L- or D-Gln, 30 seconds incubation time, and 325 nm excitation wavelength).

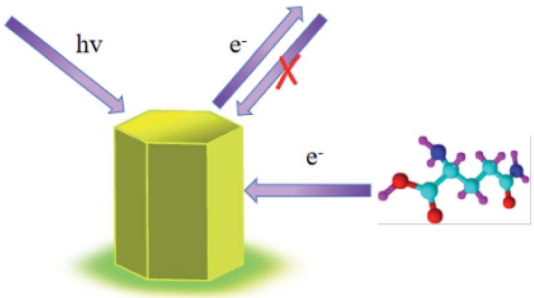

Fig. 10 PET mechanism of fluorescence quenching of PCN-128Y-1 by the Gln enantiomers.

inhibited the fluorescence (Fig. 10). This process, namely PET inhibition or suppression, relied on the distance between the electron donor and the fluorophore. There were some common electron donors such as amino, amides, and thiourea.[48] PCN-128Y and PCN-128Y-1, 2, 3 were excited by the excitation energy and the adsorbed molecule Gln with amino electron-donating groups immediately occupying the electron holes, which caused the excited electrons of the MOFs to return to a higher energy level, thereby achieving the inhibitory effect of Gln on the fluorescence of the MOFs.

There was one more point that compared with the other MOFs in this experiment, PCN-128Y-1 showed the best chiral recognition ability. Based on the percentage of C, O, and Zr elements of the energy dispersive spectrum (Fig. S3 and Table S1†) and the molecular structure of PCN-128Y, per Zr_6 nodes of PCN-128Y-1, 2, 3 were linked with 1.07, 2.28, and 2.32 L-DBTarA molecules by calculation. The free terminal nodes of the Zr_6 cluster of PCN-128Y-1 were more than that of PCN-128Y-1 and PCN-128Y-2 so that the smaller inhibition of steric hindrance could enhance the interaction between the target analyte and the chiral modifier. Conversely, as the amount of the chiral modifier increased, more terminal nodes of the Zr_6 cluster were occupied so that the target analyte did not enter the holes and could not be distinguished.

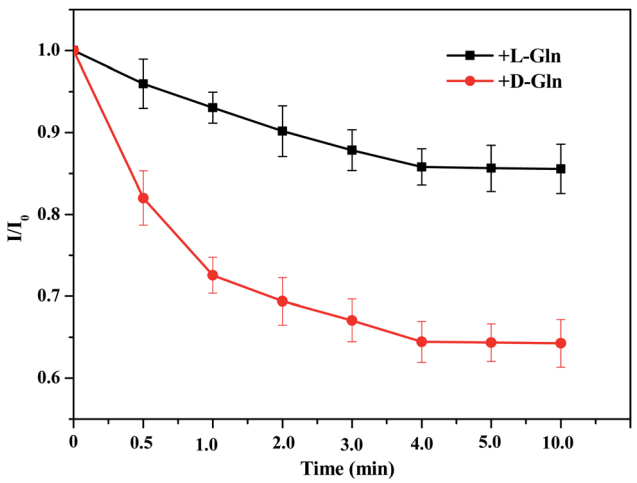

Fig. 11 The effect of incubation time on the I/I_0 of PCN-128Y-1 after adding L/D-Gln (experimental conditions: 0.05 mg mL^{-1} MOFs, 50 μL 1 mol L^{-1} L- or D-Gln, and 325 nm excitation wavelength).

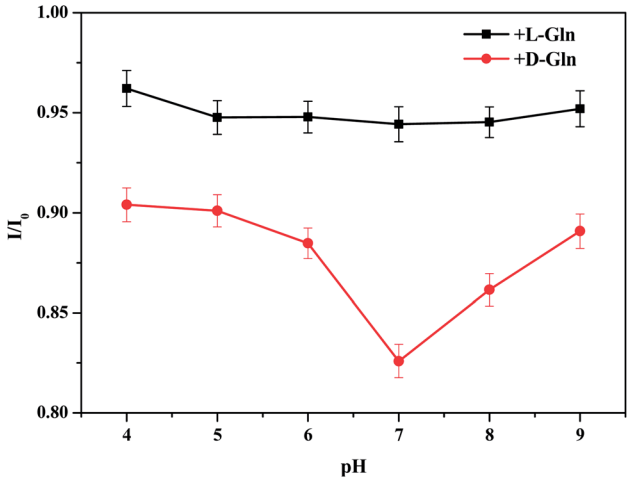

Fig. 12 The effect of pH on the I/I_0 of PCN-128Y-1 after adding D/L-Gln (experimental conditions: acetate buffer, 0.05 mg mL^{-1} MOFs, 50 μL 1 mol L^{-1} L- or D-Gln, 30 seconds incubation time, and 325 nm excitation wavelength).

Last but not least, the fluorescence quenching of PCN-128Y-1 caused by D-Gln was larger than that of L-Gln. Chiral selectivity was mainly attributed to the preferential interaction between one enantiomer and the chiral selector, which meant that the homochiral interactions were frequently stronger than the heterochiral interactions. In the PCN-128Y-1 system, L-DBTarA and D-Gln exhibited the same negative optical rotation shown in Fig. 8 so that the binding action of D-Gln and PCN-128Y-1 was greater than that of L-Gln and PCN-128Y-1 based on the spatial requirement.[49] As a consequence, PCN-128Y-1 showed good chiral selectivity toward D-Gln.

Effect of the incubation time and pH value on the chiral fluorescence recognition of PCN-128Y-1

The incubation time was investigated by the fluorescence intensity ratio (I/I_0) of PCN-128Y-1 within 0–10 min after the addition of D- and L-Gln. The results shown in Fig. 11 illustrated a decrease in the I/I_0 ratio of PCN-128Y-1 with increasing incubation time. The adsorption equilibrium was gradually reached because of the nearly unchanged I/I_0 values after 4 min. A significant difference in the I/I_0 value between D- and L-Gln was also observed when the incubation time was 30 seconds. It illustrated that PCN-128Y-1 had rapid and chiral recognition ability toward the Gln enantiomers.

The effect of the pH value on the I/I_0 values largely decides the practical application of fluorescent MOFs. The pH value of the tested solution was examined in the range from 4.0 to 9.0. As a result, in Fig. 12, no significant change in the I/I_0 value of PCN-128Y-1 quenched by L-Gln was observed with the increase in the pH value. However, the I/I_0 value of PCN-128Y-1 quenched by D-Gln reached a minimum when the pH value was equal to 7. As shown in Fig. S4,† the pH value had a strong influence on the fluorescence intensity of chiral modified PCN-128Y. It may be that the charge-compensating substitution of the chiral modifier introduced into the PCN-128Y-1 framework decreased

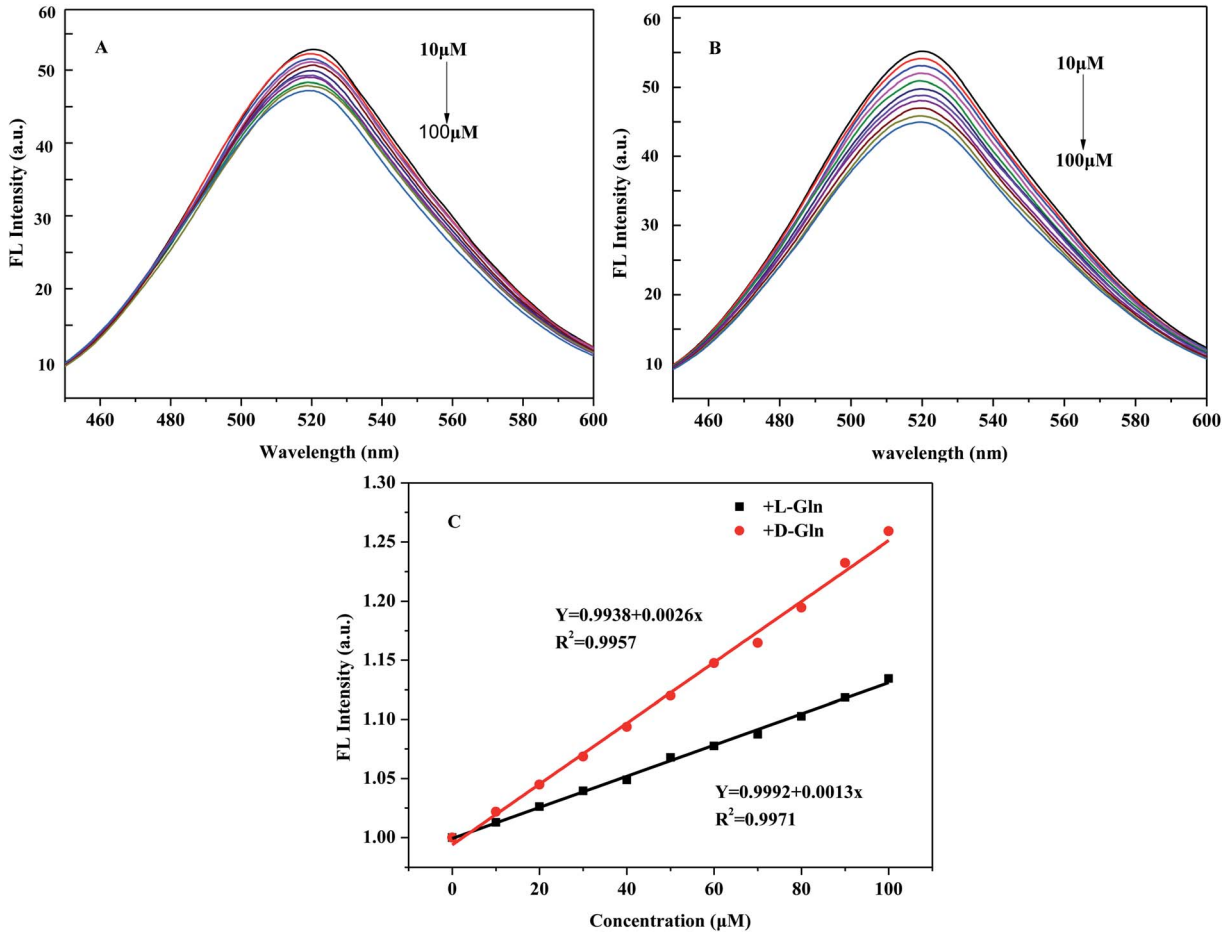

Fig. 13 Fluorescence spectra of PCN-128Y-1 quenched by different concentrations of D-Gln (A), L-Gln (B), and Stern–Volmer quenching plots for D/L-Gln (C) (experimental conditions: 0.05 mg mL^{-1} MOFs, 30 seconds incubation time, and 325 nm excitation wavelength).

under the non-neutral pH condition[33] so that the fluorescence intensity and the chiral recognition ability diminished.

Fluorescence quenching titrations of the Gln enantiomers

In order to investigate the fluorescence quenching of PCN-128Y-1 at different concentrations of the Gln enantiomers, fluorescence quenching titrations were performed with the incremental addition of D- and L-Gln to the dispersion of PCN-128Y-1 in water. As shown in Fig. 13(A) and (B), the fluorescence quenching data of D- and L-Gln could be easily analyzed by the linear regression of the Stern–Volmer equation.[50]

$$\frac{I_0}{I} = 1 + K_{SV}[Q]$$

in which I_0 and I are the fluorescence intensities of PCN-128Y-1 in the absence and presence of the analyte, respectively, K_{SV} is the quenching constant, and [Q] is the concentration of the analyte. In the concentration range of 10–100 μM, the fluorescence intensity of D- and L-Gln showed a good linear relationship, and the linear correlation coefficient (R^2) was greater than 0.99. Also, the quenching constants were $K_{SV(D)} = 2.6 \times 10^3$ L mol^{-1} and $K_{SV(L)} = 1.3 \times 10^3$ L mol^{-1}. The higher the magnitude of K_{SV}, the better the quenching process, which indicated a greater degree of exposure of the fluorophore to the quencher. Obviously, the Gln enantiomers were distinguished by PCN-128Y-1 because the K_{SV} of D-Gln was twice that of L-Gln. Meanwhile, the detection limit of D- and L-Gln was 6.6×10^{-4} mol L^{-1} and 3.3×10^{-4} mol L^{-1}, respectively, which was calculated by $3\delta/K$ (δ and K is the slope and standard deviation, respectively). The rapid chiral recognition and quantitative analysis of the Gln enantiomers were implemented using PCN-128Y-1 as the fluorescence probe.

Enantioselective fluorescence response of PCN-128Y-1 to other amino acids

Here, the enantioselectivity of PCN-128Y-1 was evaluated using the other six amino acids (Phe, Val, Ala, Pro, Tyr, and Trp) as the reference analytes. The quenching ratio (QR) was calculated by the ratio of I/I_0 for the D- and L-amino acids [*i.e.*, QR = $(I/I_0)_L/(I/I_0)_D$]. The value of QR greater than 1 indicated the advantage adsorption of PCN-128Y-1 for the D-amino acid; conversely, less than 1 favored the adsorption of the L-amino acid. On the other hand, the value of QR equal to 1 indicated that MOFs had no chiral recognition toward the amino acid enantiomers, and the results are shown in Fig. 14 and Table 3. As seen, the

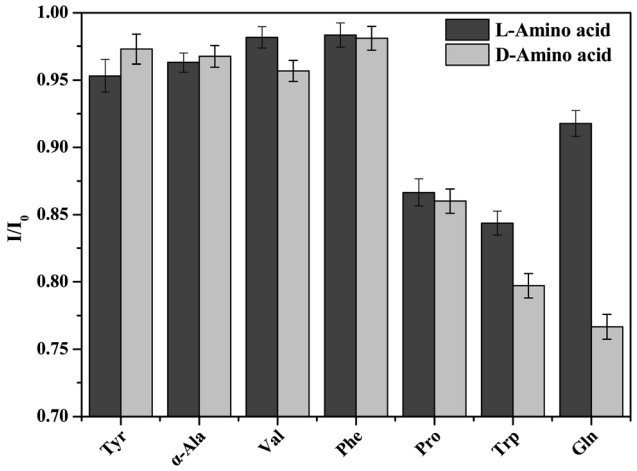

Fig. 14 The I/I_0 values of PCN-128Y-1 quenched by seven chiral acid enantiomers (experimental conditions: 0.05 mg mL^{-1} MOFs, 50 μL 1 mol L^{-1} L- or D-amino acid, 30 seconds incubation time, and 325 nm excitation wavelength).

Table 3 The quenching ratio (QR) of seven amino acids to PCN-128Y-1

	Tyr	α-Ala	Trp	Pro	Val	Phe	Gln
QR	0.98	1.00	1.01	1.01	1.03	1.00	1.20

fluorescence quenching of PCN-128Y-1 was caused by seven amino acid enantiomers because the I/I_0 values were less than 1. This was because the fluorescence of the aromatic systems in PCN-128Y-1 could be quenched by the zwitterionic forms of the amino acids based on the PET mechanism. Furthermore, PCN-128Y-1 showed very weak chiral response to the other six amino acids, compared to glutamin enantiomers with the highest QR value of 1.20. The polar functional groups and the molecule size of the adsorption substrate played a more decisive role in manifesting the enantioselectivity of PCN-128Y-1. Because of the different side-chains, α-Ala, Trp, Pro, Val, and Phe were classified as neutral nonpolar amino acids. However, Tyr and Gln were classified as neutral polar amino acids, which were more easily adsorbed by PCN-128Y-1 with polar hydroxyl and ester groups. Compared with Tyr, Gln with minimal molecule volume and more polar groups easily entered into the chiral MOFs cavity, which could form the hydrogen bonds and steric interaction with the L-DBTarA chiral ligand, leading to a much-enhanced enantioselectivity. Moreover, L-Tyr and D-Gln had the same negative optical rotation as PCN-128Y-1. Due to the homochiral interaction, L-Tyr and D-Gln had a higher I/I_0 and greater fluorescence response toward PCN-128Y-1.[51]

Adsorption properties of PCN-128Y-1

Adsorption isotherms. To investigate the adsorption performances of PCN-128Y-1, binding experiments were carried out in a series of aqueous solutions. The corresponding standard curves of L- and D-Gln are shown in Fig. S5.† It could also be

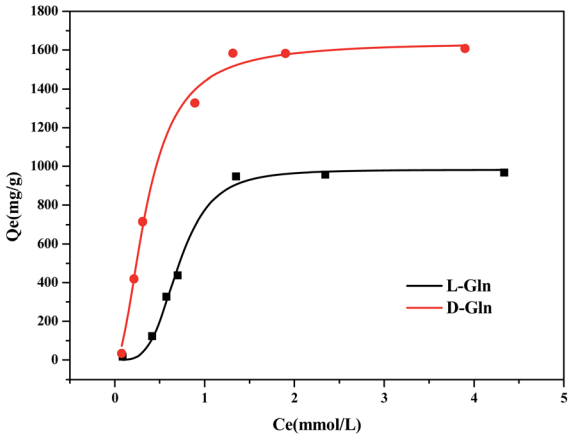

Fig. 15 Langmuir fitting adsorption isotherm of D- and L-Gln in PCN-128Y-1 (experimental conditions: 1 mg mL^{-1} MOFs, 12 h incubation time, and 214 nm absorption wavelength).

observed in Table S2† that the linear relationship between the absorbance and the concentration (0.1–5.0 mmol L^{-1}) was good, and the correlation coefficients (R^2) of the curves were greater than 0.99, which could be used for the next quantitative analysis experiment. Meanwhile, the adsorption isotherms (Fig. 15) showed that with an increase in the equilibrium concentrations of the Gln enantiomers, the equilibrium adsorption capacity (Q_e) of PCN-128Y-1 increased. The maximum capacities of PCN-128Y-1 for D-Gln ($Q_{e(D\text{-}Gln)}$ = 1607 mg g^{-1}) were 1.66 times for L-Gln ($Q_{e(L\text{-}Gln)}$ = 967 mg g^{-1}), indicating that PCN-128Y-1 had strong adsorption capacity toward the Gln enantiomers and higher affinity for D-Gln.

In addition, the common Langmuir isotherm model was used to analyze the adsorption data and is represented as follows.[52]

$$\frac{C_e}{Q_e} = \frac{1}{Q_m K} + \frac{C_e}{Q_m}$$

where Q_m is the maximum adsorption capacity (mg g^{-1}) and K is the Langmuir constant (L g^{-1}) related to the free energy of adsorption. From the linearly dependent coefficient of the fitted equations in Table 4, the Langmuir isotherm model fit the equilibrium data and the theoretically calculated equilibrium adsorption capacity was nearly the same as the measured one.

Table 4 Langmuir isotherm parameters for the adsorption of L-Gln and D-Gln

Sample	Eqn (1)	R^2	K (L g^{-1})	Q_m (mg g^{-1})
L-Gln	$Y^b = 1.02 \times 10^{-3}X^a + 2.74 \times 10^{-4}$	0.99	3.71	982.50
D-Gln	$Y^b = 6.09 \times 10^{-4}X^a + 8.51 \times 10^{-5}$	0.99	7.17	1639.48

[a] The equilibrium adsorption concentration of L- or D-Gln. [b] The molar ratio of the equilibrium adsorption concentration/adsorption capacity of L- or D-Gln.

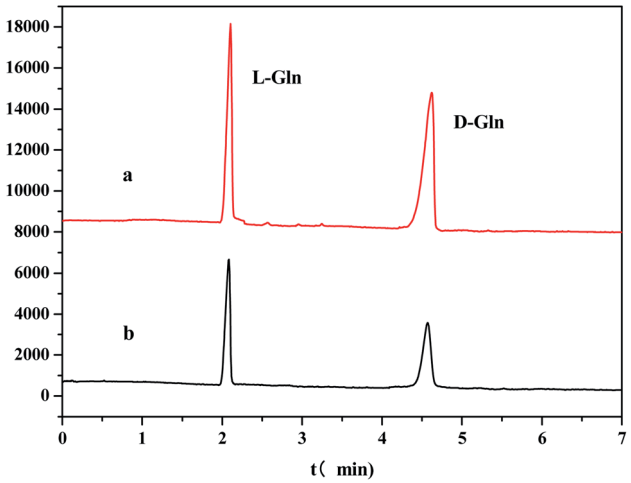

Fig. 16 CE separation diagram of the mixed solution of the Gln enantiomer ((a) D/L-Gln mixed solution before adsorption; (b) supernatant of D/L-Gln mixed solution after adsorption; experimental conditions: 15 mmol L^{-1} hydroxypropyl-β-cyclodextrin, pH = 7 20 mmol L^{-1} phosphate buffer solution, 20 kV separation voltage, and 30 °C column temperature).

Table 5 Electrophoretic separation peak area and e.e.% value of the D/L-Gln mixed solution before and after adsorption

Sample	Peak area	e.e.%
L-Gln[a]	755.3	0.2%
D-Gln[a]	758.9	
L-Gln[b]	419.1	6.2%
L-Gln[b]	370.8	

[a] The peak area before adsorption. [b] The peak area after adsorption.

These results manifested that the relatively homogeneous adsorption occurred on the surface of PCN-128Y-1. Furthermore, the higher Langmuir constant of D-Gln compared with of L-Gln also proved the superior selectivity of PCN-128Y-1 toward D-Gln.

Selective adsorption

In this study, it was found that PCN-128Y-1 not only showed rapid chiral fluorescence recognition performance but also displayed selective adsorption through the mixed isoconcentration solution of the Gln enantiomers. Therefore, the e.e.% value was measured by the capillary electrophoresis method using hydroxypropyl-β-cyclodextrin as the chiral additive. As shown in Fig. 16 and Table 5, the chromatographic peak area of D-Gln significantly reduced after the adsorption of PCN-128Y-1, and the e.e.% value was 6.2%, which revealed that the adsorption of PCN-128Y-1 was highly selective toward D-Gln.

Conclusion

In summary, a chiral fluorescent porous MOFs system was successfully devised, in which the chiral modifier L-DBTarA was rationally designed to be introduced into Zr-MOF (PCN-128Y) by the SALI method. PCN-128Y-1, as a highly sensitive fluorescent sensor, has some characteristics such as the regular six-prismatic morphology, high crystallinity, thermal stability, and negative optical rotation. Furthermore, PCN-128Y-1 exhibited higher chiral affinity for D-Gln based on the hetero-chiral interaction theory and the excellent enantioselectivity for Gln amongst seven chiral amino acids, with a QR of 1.2, under the conditions of neutral aqueous solution for 30 seconds. PCN-128Y-1 has proved to be an invaluable functional MOFs, both as a specific chiral selective adsorbent and as a chiral fluorescence sensor, which could provide the possibility of using this technique for the selective and quantitative analysis of the Gln enantiomers.

Conflicts of interest

There are no conflicts to declare.

Acknowledgements

We gratefully acknowledge the support of the basic special engineering general program of Heilongjiang Provincial Education Department (No. 135409205) and the Students Innovation and Entrepreneurship Training Program of Heilongjiang Province (No. 202110232093).

References

1 R. Bentley, *Chem. Soc. Rev.*, 2005, **34**, 609–624.
2 B. E. Weiss-López, M. Azocar, R. Montecinos, B. K. Cassels and R. Araya-Maturana, *Langmuir*, 2001, **17**, 6910–6914.
3 H. Z. Zhang, L. Qi, L. Q. Mao and Y. Chen, *J. Sep. Sci*, 2012, **35**, 1236–1248.
4 H. Q. Cao, J. K. Li, F. G. Zhang, D. Cahard and J. A. Ma, *Adv. Synth. Catal.*, 2020, **363**, 688–729.
5 E. Zor, *Talanta*, 2018, **184**, 149–155.
6 Y. P. Xue, C. H. Cao and Y. G. Zheng, *Chem. Soc. Rev.*, 2018, **47**, 1516–1561.
7 X. X. Zhang, L. Gao, Z. J. Zhang and Y. Tian, *J. Pharm. Anal.*, 2017, **7**, 303–308.
8 J. M. Mates, J. A. Segura and A. Jose, *Int. J. Biochem. Cell Biol.*, 2009, **41**, 2051–2061.
9 J. L. Coloff, J. P. Murphy, C. R. Braun, I. S. Harris, L. M. Shelton, K. Kami, S. P. Gygi, L. M. Selfors and J. S. Brugge, *Cell Metab.*, 2016, **23**, 867–880.
10 S. Staden-van, R. M. Ilie-Mihai, L. Magerusan, M. Coros and S. Pruneanu, *Anal. Bioanal. Chem.*, 2020, **412**, 13.
11 E. Zor, H. Bingol and M. Ersoz, *TrAC, Trends Anal. Chem.*, 2019, **121**, 115662–115679.
12 X. He, Q. Zhang, W. Wang, L. Lin, X. Liu and X. Feng, *Org. Lett.*, 2011, **13**, 804–807.
13 H. Hwa Jo, C. Lin and E. V. Anslyn, *Acc. Chem. Res.*, 2014, **47**, 2212–2221.
14 D. Leung, S. O. Kang and E. V. Anslyn, *Chem. Soc. Rev.*, 2012, **41**, 448–479.
15 A. Accetta, R. Corradini and R. Marchelli, *Top. Curr. Chem.*, 2011, **300**, 175–216.

16 L. A. Joyce, S. H. Shabbir and E. V. Anslyn, *Chem. Soc. Rev.*, 2010, **39**, 3621–3632.
17 J. R. Li, Y. Ma, M. C. McCarthy, J. Sculley, J. M. Yu, H. K. Jeong, P. B. Balbuena and H. C. Zhou, *Coord. Chem. Rev.*, 2011, **255**, 1791–1823.
18 J. R. Li, R. J. Kuppler and H. C. Zhou, *Chem. Soc. Rev.*, 2009, **38**, 1477–1504.
19 J. Lee, O. K. Farha, J. Roberts, K. A. Scheidt, S. T. Nguyen and J. T. Hupp, *Chem. Soc. Rev.*, 2009, **38**, 1450–1459.
20 J. Rocha, L. D. Carlos, F. A. A. Paz and D. Ananias, *Chem. Soc. Rev.*, 2011, **40**, 926–940.
21 Z. C. Hu, B. J. Deibert and J. Ling, *Chem. Soc. Rev.*, 2014, **43**, 5815–5840.
22 W. P. Lustig, S. Mukherjee, N. D. Rudd, A. V. Desai, J. Li and S. K. Ghosh, *Chem. Soc. Rev.*, 2017, **46**, 3242–3285.
23 Y. Zhou, H. H. Chen and B. Yan, *J. Mater. Chem.A*, 2014, **2**, 13691–13697.
24 X. Y. Xu and B. Yan, *Adv. Funct. Mater.*, 2017, **27**, 1700247.
25 N. Bhardwaj, S. Bhardwaj, J. Mehta, K. H. Kim and A. Deep, *Biosens. Bioelectron.*, 2016, **86**, 799–804.
26 X. Y. Xu, X. Lian, J. N. Hao, C. Zhang and B. Yan, *Adv. Mater.*, 2017, **29**, 1702298.
27 R. B. Lin, S. Y. Liu, J. W. Ye, X. Y. Li and J. P. Zhang, *Adv. Sci.*, 2016, **3**, 1500434.
28 J. N. Hao and B. Yan, *Adv. Funct. Mater.*, 2017, **27**, 1603856.
29 Y. H. Zhang, B. Li, H. P. Ma, L. M. Zhang and Y. X. Zheng, *Biosens. Bioelectron.*, 2016, **85**, 287–293.
30 S. Y. Moon, A. J. Howarth, T. Wang, N. A. Vermeulen, J. T. Hupp and O. K. Farha, *Chem. Commun.*, 2016, **52**, 3438–3441.
31 H. L. Jiang, D. W. Feng, K. C. Wang, Z. Y. Gu, Z. W. Wei, Y. P. Chen and H. C. Zhou, *J. Am. Chem. Soc.*, 2013, **135**, 13934–13938.
32 L. Li, Y. L. Zhu, X. H. Zhou, C. D. S. Brites, D. Ananias, Z. Lin, F. A. A. Paz, J. Rocha, W. Huang and L. D. Carlos, *Adv. Funct. Mater.*, 2016, **26**, 8677–8684.
33 Q. Zhang, J. Su, D. W. Feng, Z. W. Wei, X. D. Zou and H. C. Zhou, *J. Am. Chem. Soc.*, 2015, **137**, 10064–10067.
34 Y. Zhou, Q. Yang, D. N. Zhang, N. Gan, O. P. Li and J. Cuan, *Sens. Actuators, B*, 2018, **262**, 137–143.
35 P. Deria, J. E. Mondloch, E. Tylianakis, P. Ghosh, W. Bury, R. Q. Snurr, J. T. Hupp and O. K. Farha, *J. Am. Chem. Soc.*, 2013, **135**, 16801–16804.
36 P. Deria, W. Bury, J. T. Hupp and O. K. Farha, *Chem. Commun.*, 2014, **50**, 1965–1968.
37 C. T. Lollar, J. S. Qin, J. D. Pang, S. Yuan, B. Becker and H. C. Zhou, *Langmuir*, 2018, **34**, 13795–13807.
38 G. Nickerl, A. Henschel, R. Grunker, K. Gedrich and S. Kaskel, *Chem. Ing. Tech.*, 2011, **83**, 90–101.
39 Z. L. Wu, J. Dong, W. Y. Ni, B. W. Zhang, J. Z. Cui and B. Zhao, *Inorg. Chem.*, 2015, **54**, 5266–5272.
40 J. Amaro-Gahete, D. Esquivel, J. R. Ruiz, C. Jimenez-Sanchidrian and F. J. Romero-Salguero, *Appl. Catal., A*, 2019, **585**, 117190.
41 S. L. Qin, L. Q. Su, P. Wang and S. Deng, *J. Appl. Polym. Sci.*, 2015, **132**, 41491.
42 Y. L. Chen, L. Xia, Z. C. Lu, G. K. Li and Y. L. Hu, *J. Chromatogr. A*, 2021, **1654**, 462475.
43 L. Luconi, G. Mercuri, T. Islamoglu, A. Fermi, G. Bergamini, G. Giambastiani and A. Rossin, *J. Mater. Chem. C*, 2020, **8**, 7492–7500.
44 J. S. Oh, Y. You, K. C. Park, G. Gupta, D. K. Kang and C. Y. Lee, *Dyes Pigm.*, 2019, **170**, 107576.
45 Z. H. Sun, Y. Shen and U. Niinemets, *J. Exp. Bot.*, 2020, **71**, 7364–7381.
46 R. Yoshii, A. Nagai, K. Tanaka and Y. Chujo, *Chem.–Eur. J.*, 2013, **19**, 4506–4512.
47 L. Quan, Y. Chen, X. J. Lv and W. F. Fu, *Chem.–Eur. J.*, 2012, **18**, 14599–14604.
48 F. F. Yu, Y. Chen, H. Jiang and X. M. Wang, *Analyst*, 2020, **145**, 6769–6812.
49 Y. W. Wang, X. J. Zhou, C. L. Xu, Y. Jin and B. X. Li, *Sci. Rep.*, 2018, **8**, 5296.
50 Y. S. Liu, Z. J. Chen, W. Li, C. H. Ma, P. Wu, X. Y. Wu, S. J. Li and S. X. Liu, *Microchim. Acta*, 2018, **185**, 518.
51 W. H. Stein, S. Moore and M. Bergmann, *J. Am. Chem. Soc.*, 2002, **64**, 724–725.
52 A. Li, N. X. Zheng, T. Yang, J. Xie, L. J. Li, K. W. Tang and C. S. Zhou, *RSC Adv.*, 2021, **11**, 29807–29815.